Ting Yao,[1,2] Zhuo Deng,[2,3] Yong Gao,[2,4] Jia Sun,[2,5] Xingxing Kong,[6] Yiru Huang,[2,7] Zhenyan He,[2,7] Yanchao Xu,[2] Yongsheng Chang,[4] Kai-jiang Yu,[8] Brianna G. Findley,[9] Eric D. Berglund,[9] Rui-tao Wang,[8] Hongbo Guo,[7] Hong Chen,[5] Xu Li,[10] Randal J. Kaufman,[11] Jianqun Yan,[1] Tiemin Liu,[2,8] and Kevin W. Williams[2]

Ire1α in *Pomc* Neurons Is Required for Thermogenesis and Glycemia

Diabetes 2017;66:663–673 | DOI: 10.2337/db16-0533

Whether neuronal inositol-requiring enzyme 1 (*Ire1*) is required for the proper regulation of energy balance and glucose homeostasis is unclear. We found that pro-opiomelanocortin (*Pomc*)–specific deficiency of *Ire1α* accelerated diet-induced obesity concomitant with a decrease in energy expenditure. This hypometabolic phenotype included deficits in thermogenic responses to diet and cold exposure as well as "beiging" of white adipose tissue. We also demonstrate that loss of *Ire1α* in *Pomc* neurons impaired whole-body glucose and insulin tolerance as well as hepatic insulin sensitivity. At the cellular level, deletion of *Ire1α* in *Pomc* neurons elevated hypothalamic endoplasmic reticulum (ER) stress and predisposed *Pomc* neurons to leptin and insulin resistance. Together, the current studies extend and confirm conclusions that *Ire1α-Xbp1s* and associated molecular targets link ER stress in arcuate *Pomc* neurons to aspects of normal energy and glucose homeostasis.

Obesity and diabetes remains one of the leading causes of death in developed countries. Importantly, a variety of metabolic abnormalities have been linked to endoplasmic reticulum (ER) stress and the unfolded protein response (UPR) (1–3). In particular, genetically obese mice exhibit ER stress and activation of the UPR in the periphery as well as in the central nervous system (CNS) (4,5). Moreover, nutrient-dependent regulation of the UPR has been suggested to be a major contributor to diet-induced metabolic dysfunction within the periphery as well as the brain (4,6–8).

The inositol-requiring enzyme 1/X-box binding protein 1 (*Ire1-Xbp1*) pathway is the most conserved of the three branches of the UPR (9–13). Activated Ire1 exhibits endoribonuclease activity, which cleaves its primary target, the mRNA encoding *Xbp1*, and generates a potent transcription factor that stimulates expression of chaperones and components of the ER-associated protein degradation pathway (9). Although global deletion of *Ire1* or *Xbp1* in mice produces an embryonic lethal phenotype (14–16), neuronal deletion of *Xbp1* creates severe ER stress in the hypothalamus, blocks leptin action, and generates leptin resistance in mice (4). (Note that Xbp1 deletion causes Ire1 hyperactivation, which leads to cell death.) Similarly, chemical activation of ER stress in pro-opiomelanocortin (*Pomc*) neurons results in acute leptin

[1]Department of Physiology and Pathophysiology, School of Basic Medical Sciences, Xi'an Jiaotong University School of Medicine, Xi'an, Shaanxi, China
[2]Division of Hypothalamic Research, Department of Internal Medicine, University of Texas Southwestern Medical Center, Dallas, TX
[3]Department of Gynecology, Shaanxi Provincial People's Hospital, Shaanxi, China
[4]National Laboratory of Medical Molecular Biology, Institute of Basic Medical Sciences, Chinese Academy of Medical Sciences and Peking Union Medical College, Beijing, China
[5]Department of Endocrinology, Zhujiang Hospital, Southern Medical University, Guangzhou, China
[6]Division of Endocrinology, Beth Israel Deaconess Medical Center and Harvard Medical School, Harvard University, Boston, MA
[7]Department of Neurosurgery, Zhujiang Hospital, Southern Medical University, Guangzhou, China
[8]Department of Intensive Care Unit, Third Affiliated Hospital, Harbin Medical University, Harbin, China
[9]Division of Metabolic Mechanisms of Disease, Advanced Imaging Research Center and Department of Pharmacology, University of Texas Southwestern Medical Center, Dallas, TX
[10]Department of Obstetrics and Gynecology, First Affiliated Hospital, Xi'an Jiaotong University School of Medicine, Xi'an, Shaanxi, China
[11]Degenerative Diseases Program, Sanford Burnham Prebys Medical Discovery Institute, La Jolla, CA

Corresponding authors: Kevin W. Williams, kevin.williams@utsouthwestern.edu, Tiemin Liu, tiemin.liu@utsouthwestern.edu, and Jianqun Yan, jqyan@xjtu.edu.cn.

Received 27 April 2016 and accepted 16 December 2016.

T.Y., Z.D., Y.G., and J.S. are co-first authors.

This article includes Supplementary Data online at http://diabetes.diabetesjournals.org/lookup/suppl/doi:10.2337/db16-0533/-/DC1.

and insulin resistance via a *Ptp1b*- and *Socs3*-dependent mechanism (17). Importantly, constitutive activation of the spliced isoform of Xbp1 (*Xbp1s*) in *Pomc* neurons mimics a postprandial state, resulting in improved body weight and decreased glucose and insulin levels (17).

Although driving the *Ire1-Xbp1s* pathway in arcuate *Pomc* neurons is sufficient to improve body weight and glucose homeostasis, the requirement of this highly conserved pathway in *Pomc* neurons to regulate metabolism remains to be established. We therefore tested the hypothesis that *Ire1* signaling in *Pomc* neurons is necessary for proper energy balance and glucose metabolism.

RESEARCH DESIGN AND METHODS

Animal Care

Pomc-cre (25) and *Ire1α*$^{fe/fe}$ (20) mice were group housed (1–5 mice per cage) in a barrier facility at 23°C unless otherwise noted. Male mice in a C57Bl/6 background were used for all studies. Mice were provided a Harlan Teklad 2016 chow diet and water ad libitum unless otherwise noted. Mice were placed on a high-fat/high-sucrose (HFHS; Research Diets D12331) diet at 8 weeks of age, if applicable, and HFHS diet was removed and refilled weekly. Mice losing >10% of body weight during the acclimation period for metabolic cage studies (see below) were not studied. Body composition was measured using nuclear magnetic resonance (Bruker minispec).

Metabolic Cages

Experiments were performed in a temperature-controlled room containing 36 TSE metabolic cages maintained by University of Texas Southwestern (UTSW) Animal Resources personnel. One week prior to study, mice were singly housed to acclimate to new housing. Three days prior to study, mice were transported to the room containing the metabolic cages to acclimate to a new environment. HFHS diet, if applicable, was also introduced at the beginning of this acclimation period. After 3 days acclimation, cages were connected to the TSE system for a total of 5 days. Days 2–4 were used for data analyses.

Cold Exposure

Mice were housed in cold chambers maintained at 6°C by UTSW Animal Resources personnel.

Immunohistochemistry

Sixteen-week-old male mice were anesthetized and transcardially perfused with a modified ice-cold artificial cerebrospinal fluid (ACSF) (126 mmol/L NaCl, 2.8 mmol/L KCl, 1.2 mmol/L $MgCl_2$, 2.5 mmol/L $CaCl_2$, 1.25 mmol/L NaH_2PO_4, 26 mmol/L $NaHCO_3$, and 5 mmol/L glucose), in which an equiosmolar amount of sucrose was substituted for NaCl. The mice were then decapitated, and the entire brain was removed and immediately submerged in ice-cold, carbogen-saturated (95% O_2 and 5% CO_2) ACSF. Coronal sections (250 μm) were cut with a Leica VT1000S vibratome and then incubated in oxygenated ACSF with tunicamycin (35 μmol/L) for 6 h. The slices were fixed by 10% neutral-buffered formalin for 4 h at room temperature and cryopreserved in 30% sucrose at 4°C overnight. Brain slices were then sectioned into 25-μm coronal sections and stored in cryoprotectant at −20°C until use. Brain sections were rinsed with PBS five times for 5 min and incubated with primary antibody (Ireα, NB100-2323, 1:100 diluted in 3% normal donkey serum, PBS and tween–azide) at 4°C overnight. Sections were then rinsed in PBS and incubated with secondary antibody (1:200 diluted in 3% normal donkey serum, PBS and tween) at room temperature for 2 h. Cells were visualized using a Zeiss microscope by an observer that was blinded to the condition or genotype of the mice.

Protein Extraction and Western Blot Analysis

Protein was extracted from brown adipose tissue (BAT) by using RIPA buffer (Boston BioProducts) supplemented with complete protease inhibitor cocktail (Roche). For Western blot analyses, 80 μg protein was subjected to SDS-PAGE under reducing conditions, transferred, and blotted with the anti-UCP1 antibody (ab10983; Abcam).

Glucose Tolerance Tests

After an overnight fast, 10- to 14-week-old male mice received intraperitoneal injections of 1.5 g/kg D-glucose. Blood glucose was measured from tail blood using a glucometer at serial time points as indicated in figures. A separate cohort of mice was used for glucose-stimulated insulin secretion (GSIS). Blood was collected at 0 and 30 min after glucose administration. Blood samples were centrifuged, and serum samples were collected from the supernatants. Insulin levels were measured using an ELISA kit (Crystal Chem Inc., Downers Grove, IL) according to the manufacturer's instruction.

Insulin Tolerance Tests

After a 4-h fast to empty the stomach, 10- to 14-week-old male mice received intraperitoneal injections of insulin (1.2 units/kg for chow-fed mice or 1.4 units/kg for high-fat diet [HFD]–fed mice). Blood glucose was measured from tail blood as described above.

Pyruvate Tolerance Tests

After a 6-h fast to empty the stomach, 10- to 14-week-old male mice received intraperitoneal injections of 2 mg/kg pyruvate. Blood glucose was measured from tail blood as described above.

Histology

Tissues were dissected and fixed in formalin for 48 h at 4°C followed by 50% ethanol. BAT histology was performed with assistance from the UTSW Histology Core. Inguinal white adipose tissue (iWAT) was performed with assistance from the Harvard Histology Core.

Electrophysiology

Whole-cell patch-clamp recordings from Pomc-hrGFP (humanized, *Renilla reniformis* green fluorescent protein) neurons maintained in hypothalamic slice preparations and data analysis were performed as previously described (17,18). In brief, 4- to 16-week-old male mice were anesthetized and transcardially perfused with a modified ice-cold

ACSF (described below), in which an equiosmolar amount of sucrose was substituted for NaCl. The mice were then decapitated, and the entire brain was removed and immediately submerged in ice-cold, carbogen-saturated (95% O_2 and 5% CO_2) ACSF (126 mmol/L NaCl, 2.8 mmol/L KCl, 1.2 mmol/L $MgCl_2$, 2.5 mmol/L $CaCl_2$, 1.25 mmol/L NaH_2PO_4, 26 mmol/L $NaHCO_3$, and 5 mmol/L glucose). Coronal sections (250 μm) were cut with a Leica VT1000S vibratome and then incubated in oxygenated ACSF at room temperature for at least 1 h before recording. Slices were transferred to the recording chamber and allowed to equilibrate for 10–20 min before recording. The slices were bathed in oxygenated ACSF (32°C–34°C) at a flow rate of ~2 mL/min.

The pipette solution for whole-cell recording was modified to include an intracellular dye (Alexa Fluor 594 or Alexa Fluor 350) for whole-cell recording: 120 mmol/L K-gluconate, 10 mmol/L KCl, 10 mmol/L HEPES, 5 mmol/L EGTA, 1 mmol/L $CaCl_2$, 1 mmol/L $MgCl_2$, and 2 mmol/L MgATP and either 0.03 mmol/L Alexa Fluor 594 or Alexa Fluor 350 hydrazide dye (pH 7.3). Epifluorescence was briefly used to target fluorescent cells, at which time the light source was switched to infrared differential interference contrast imaging to obtain the whole-cell recording (Zeiss Axioskop FS2 Plus equipped with a fixed stage and a QuantEM:512SC electron-multiplying charge-coupled device camera). Electrophysiological signals were recorded using an Axopatch 700B amplifier (Molecular Devices), low-pass filtered at 2–5 kHz, and analyzed offline on a PC with pCLAMP programs (Molecular Devices). Recording electrodes had resistances of 2.5–5 mol/LΩ when filled with the K-gluconate internal solution. Input resistance was assessed by measuring voltage deflection at the end of the response to a hyperpolarizing rectangular current pulse step (500 ms of −10 to −50 pA).

Leptin (100 nmol/L, provided by A.F. Parlow through the National Hormone and Peptide Program, Harbor-UCLA Medical Center, Torrance, CA) or insulin (50 nmol/L, Humulin R 100 units/mL; Eli Lilly and Company) was added to the ACSF for specific experiments. Solutions containing leptin or insulin were typically perfused for 2–4 min. A drug effect was required to be associated temporally with peptide application, and the response had to be stable within a few minutes. A neuron was considered depolarized or hyperpolarized if a change in membrane potential was at least 2 mV in amplitude.

Analysis of Gene Expression by Quantitative PCR

A coronal slice between bregma –1.22 and –2.70 mm was made from age- and weight-matched mice, and then the arcuate nucleus was microdissected with a scalpel under a microscope. Total RNA was extracted from tissues with TRIzol reagent (Invitrogen) according to the manufacturer's instructions. Total RNA (1 μg) was converted into first-strand cDNA with oligo(dT) primers as described by the manufacturer (Clontech). PCR was performed in an Mx3000P Q-PCR system (Stratagene) with specific primers and SYBR Green PCR Master Mix (Stratagene). The relative abundance of mRNAs was standardized with 18S mRNA as the invariant control.

Hyperinsulinemic-Euglycemic Clamps

Experiments were done in conscious, chronically catheterized mice using previously described techniques (17). After a 5-day recovery, food was removed on day of experiment at 0800 h to begin a 5-h fast. [3,4-$^{13}C_2$]glucose (Cambridge Isotopes) was infused beginning at t = –120 min to calculate glucose turnover. Humulin R (2.5 mU/kg/min) was then infused at t = 0 min to induce hyperinsulinemia. Blood samples from the cut tail were taken every 10 min, and dextrose (50%) was infused as needed to maintain target blood glucose levels (~150 mg/dL).

Statistics

Statistical analysis was performed using GraphPad. All data were evaluated using a two-tailed Student t test, with a P value of <0.05 considered significant. In all instances, data are presented as mean ± SEM. Body weight curves were compared using a linear regression analysis. Degrees of freedom (DF) for t statistics are marked as $t_{(DF)}$. For

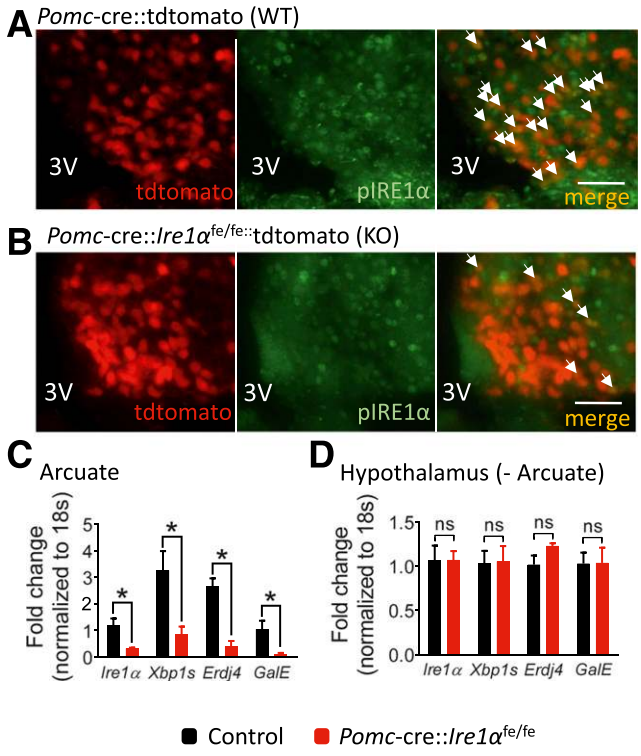

Figure 1—*Pomc*-specific deficiency of *Ire1α* in the arcuate nucleus. *A* and *B*: The phosphorylation level of Ire1 (Ser724) in Pomc neurons was measured by immunohistochemistry both in the *Pomc*-cre::tdtomato and *Pomc*-cre::*Ire1α*$^{fe/fe}$::tdtomato mice. Arrows indicate Pomc neurons expressing p*Ire1α*. Scale bars, 50 μm. *C* and *D*: qPCR was performed on *Pomc*-cre::*Ire1α*$^{fe/fe}$ mice and their littermate controls to examine the relative expression of *Ire1α*, *Xbp1s*, *Erdj4*, and *GalE*. *P < 0.05 compared with control (wild-type littermates). Fold change is relative to 18S mRNA. n = 4–8 per group. Error bars indicate SEM.

glucose tolerance test, insulin tolerance test, and pyruvate tolerance test (PTT), data were analyzed consistent with current recommendations (19,20).

Pre-established criteria for excluding data points were data two SDs outside the mean or any data obtained from mice that died or lost >10% of body weight due to metabolic cage acclimation or clamp studies.

RESULTS

Pomc-Specific Deficiency of *Ire1α* Accelerates Diet-Induced Obesity

The downstream target of *Ire1α*, *Xbp1s*, improves energy expenditure and glucose metabolism in the periphery as well as the CNS (4,5,17,21,22). In particular, we recently demonstrated that overexpression of *Xbp1s* in *Pomc* neurons alone was sufficient to protect against diet-induced obesity as well as glucose and insulin intolerance (17). In order to test the requirement of the *Ire1-Xbp1s* arm of the UPR in *Pomc* neurons to regulate body weight, we generated mice that were deficient for *Ire1α* specifically in *Pomc* neurons, *Pomc*-cre::*Ire1α*$^{fe/fe}$ mice (23). Fluorescent immunohistochemistry demonstrated that p*Ire1α* can be detected in the arcuate nucleus (Fig. 1). The cells expressing p*Ire1α* include those identified as *Pomc* neurons as visible by tdtomato expression (Fig. 1*A*). Notably, Pomc neurons deficient for *Ire1α* (*Pomc* neurons from *Pomc*-cre::*Ire1α*$^{fe/fe}$ mice) exhibit a reduced expression of p*Ire1α* (Fig. 1*B*). Similar data were obtained with quantitative PCR (qPCR) from arcuate punches (Fig. 1*C*). As expected, *Pomc*-cre::*Ire1α*$^{fe/fe}$ mice displayed diminished mRNA for *Xbp1s* as well as the putative target genes of Xbp1s (*Erdj4* and *GalE*) in the arcuate nucleus (for *Xbp1s*: $t_{(11)} = 2.507$, $P < 0.05$; for *Erdj4*: $t_{(4)} = 6.645$, $P < 0.05$; for *GalE*: $t_{(4)} = 3.891$, $P < 0.05$) (Fig. 1*C*). However, we failed to detect alterations of ER stress markers and putative downstream targets for *Xbp1s* outside the arcuate nucleus between control and *Pomc*-cre::*Ire1α*$^{fe/fe}$ mice (Fig. 1*D*). These data support a Pomc-specific downregulation of Ire1α expression in mice selectively deficient for Ire1α in *Pomc*-cre::*Ire1α*$^{fe/fe}$ mice.

On a chow diet, *Pomc*-cre::*Ire1α*$^{fe/fe}$ mice displayed similar body weight to littermate controls (Fig. 2*A*). However when fed an HFD, male *Pomc*-cre::*Ire1α*$^{fe/fe}$ mice exhibit an age-dependent increased body weight compared with wild-type mice (Fig. 2*B*), which was reflected by increased fat mass ($t_{(10)} = 3.171$, $P < 0.05$) (Fig. 2*C*). Age- and weight-matched *Pomc*-cre::*Ire1α*$^{fe/fe}$ male mice had increased caloric intake and were hypometabolic, as demonstrated by significantly increased food intake and decreased energy expenditure (Fig. 2*D–J*). *Pomc*-cre::*Ire1α*$^{fe/fe}$ mice were also less sensitive to acute leptin-induced hypophagia when compared with littermate controls at 1 h after refeeding (Fig. 2*K*).

Several studies have suggested that melanocortin neurons regulate intrascapular BAT (iBAT), which is a key component of adaptive thermogenesis (17,24,25).

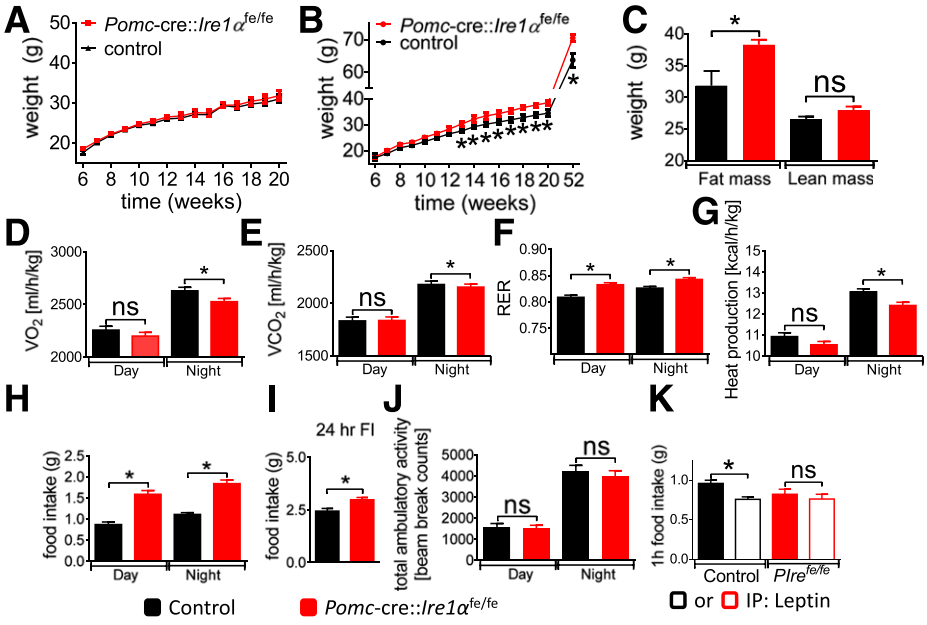

Figure 2—Body weight and metabolic assessment of male wild-type and *Pomc*-cre::*Ire1α*$^{fe/fe}$ mice. Body weight curve of male *Pomc*-cre::*Ire1α*$^{fe/fe}$ mice on a chow diet (*A*) or an HFD (*B*) (*$P < 0.05$). *C*: Body fat composition of male mice on an HFD at 52 weeks (*$P < 0.05$). *D–J*: Male *Pomc*-cre::*Ire1α*$^{fe/fe}$ mice were placed on an HFD at 8 weeks of age. Mice displayed decreased VO_2 (*D*), decreased VCO_2 (*E*), increased respiratory exchange ratio (RER) (*F*), decreased heat production (*G*), and increased food intake (FI) both in day/night cycles (*H*) and over 24 h (*I*), with no change in ambulatory activity (*J*). Error bars indicate SEM. Mice used in *D–J* were age-matched male littermates (8–12 weeks of age) and had comparable body weight and lean mass. For *D–J*, $n = 12–14$ per group; *$P < 0.05$. *K*: Leptin-induced hypophagia was observed at 1 h after refeeding in control mice. *Pomc*-cre::*Ire1α*$^{fe/fe}$ mice failed to demonstrate hypophagia in response to pharmacological administration of oral (o) or intraperitoneal (IP) leptin (open squares) at 1 h after refeeding. IP, intraperitoneal. $n = 9$ per group; *$P < 0.05$.

Components of adaptive "nonshivering" thermogenesis include coordinated neuroendocrine responses to the energy demands of an HFD as well as cold exposure. Even though chow-fed *Pomc*-cre::*Ire1α*$^{fe/fe}$ mice failed to exhibit alterations in body weight, we found that transcripts associated with heat production were reduced in BAT from *Pomc*-cre::*Ire1α*$^{fe/fe}$ mice (Fig. 3*A*). Similar to previous reports, control mice fed an HFD displayed increased markers of heat production in BAT (Fig. 3*A*). However, this was not the case in BAT from *Pomc*-cre::*Ire1α*$^{fe/fe}$ littermates (Fig. 3*A*). Moreover, analyses of BAT histology after 12–24 h at 6°C demonstrated impaired thermogenic responses in *Pomc*-cre::*Ire1α*$^{fe/fe}$ mice (Fig. 3*B*). In addition, iWAT in cold-exposed *Pomc*-cre::*Ire1α*$^{fe/fe}$ mice failed to show evidence of "browning" based on histology (Fig. 3*B*) or protein expression (Fig. 3*C*). Together, these data suggest that *Ire1α* in *Pomc* neurons is essential for adaptive thermogenesis including recruitment of BAT and browning of iWAT.

Mice Lacking *Ire1α* in *Pomc* Neurons Have Impaired Insulin Sensitivity and Glycemia

Along with the systemic effects on whole-body energy expenditure and body weight, deficiency of *Ire1α* in *Pomc* neurons also leads to alterations in glucose metabolism. In particular, *Pomc*-cre::*Ire1α*$^{fe/fe}$ mice showed impaired glucose tolerance independent of diet when compared with littermate controls ($P < 0.05$) (Fig. 4*A* and *D*). *Pomc*-cre::*Ire1α*$^{fe/fe}$ mice were also insulin intolerant ($P < 0.05$) (Fig. 4*B* and *E*). Although serum insulin was only modestly increased, GSIS was increased 30 min after a glucose load ($t_{(20)} = 2.244$, $P < 0.05$) (Supplementary Fig. 1).

Mammals maintain euglycemia within a very tight range, largely dependent upon glucose production and/or secretion from the liver. The livers of chow-fed *Pomc*-cre::*Ire1α*$^{fe/fe}$ mice displayed elevated gluconeogenic markers (for *Foxo1*: $t_{(6)} = 2.883$, $P < 0.05$; for *HNF4α*: $t_{(6)} = 5.562$, $P < 0.05$; for *Pcx*: $t_{(6)} = 3.993$, $P < 0.05$; for *G6pc*: $t_{(6)} = 4.648$, $P < 0.05$; for *Pepck*: $t_{(6)} = 3.160$, $P < 0.05$) (Fig. 4*G*). Moreover, when pyruvate was provided as a fuel source (PTT), chow-fed *Pomc*-cre::*Ire1α*$^{fe/fe}$ mice displayed increased serum glucose levels (Fig. 4*C* and *F*), supportive of increased glucose production capacity within the liver.

We next performed hyperinsulinemic-euglycemic clamps to assess whether insulin sensitivity was altered in chow-fed *Pomc*-cre::*Ire1α*$^{fe/fe}$ mice versus wild-type littermates of similar body weight (Fig. 5*A*). Plasma insulin was elevated similarly in both groups (Fig. 5*B*) and blood glucose was clamped at target levels (~150 mg/dL) (Fig. 5*C*) using an

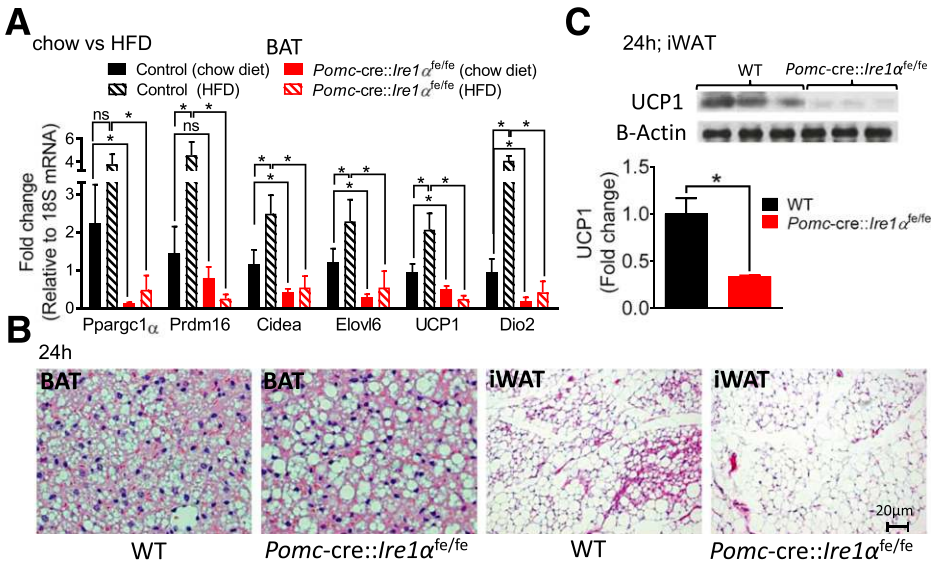

Figure 3—Deletion of *Ire1α* in *Pomc* neurons impairs BAT function and cold tolerance. *A*: *Pomc*-cre::*Ire1α*$^{fe/fe}$ mice and wild-type littermates were fed a chow diet or an HFD. qPCR was performed to examine the relative expression of *Ppargc1α*, *Prdm16*, *UCP1*, *Cidea*, *Dio2*, and *Elovl6*, which are genes associated with heat production in BAT. For comparisons between wild type (WT) mice on a chow diet and *Pomc*-cre::*Ire1α*$^{fe/fe}$ mice on a chow diet (for *Ppargc1α*: $t_{(11)} = 2.698$, $P < 0.05$; for *Prdm16*: $t_{(11)} = 0.9525$, $P > 0.05$; for *UCP1*: $t_{(11)} = 2.227$, $P < 0.05$; for *Cidea*: $t_{(11)} = 2.411$, $P < 0.05$; for *Dio2*: $t_{(11)} = 2.663$, $P < 0.05$; for *Elovl6:* $t_{(11)} = 2.924$, $P < 0.05$). For comparisons between WT mice on an HFD and *Pomc*-cre::*Ire1α*$^{fe/fe}$ mice on an HFD (for *Ppargc1α*: $t_{(15)} = 2.264$, $P < 0.05$; for *Prdm16*: $t_{(15)} = 2.306$, $P < 0.05$; for *UCP1*: $t_{(15)} = 2.543$, $P < 0.05$; for *Cidea*: $t_{(15)} = 2.179$, $P < 0.05$; for *Dio2*: $t_{(15)} = 2.715$, $P < 0.05$; for *Elovl6*: $t_{(15)} = 1.717$, $P > 0.05$). For comparisons between WT mice on a chow diet and WT mice on an HFD (for *Ppargc1α*: $t_{(10)} = 1.188$, $P > 0.05$; for *Prdm16*: $t_{(10)} = 2.661$, $P < 0.05$; for *UCP1*: $t_{(10)} = 2.162$, $P < 0.05$; for *Cidea*: $t_{(10)} = 2.912$, $P < 0.05$; for *Dio2*: $t_{(10)} = 5.090$, $P < 0.05$; for *Elovl6*: $t_{(10)} = 2.825$, $P < 0.05$). For comparisons between *Pomc*-cre::*Ire1α*$^{fe/fe}$ mice on a chow diet and *Pomc*-cre::*Ire1α*$^{fe/fe}$ mice on an HFD (for *Ppargc1α*: $t_{(12)} = 1.146$, $P > 0.05$; for *Prdm16*: $t_{(12)} = 1.555$, $P > 0.05$; for *UCP1*: $t_{(12)} = 1.762$, $P > 0.05$; for *Cidea*: $t_{(12)} = 0.4648$, $P > 0.05$; for *Dio2*: $t_{(12)} = 0.8777$, $P < 0.05$; for *Elovl6*: $t_{(12)} = 0.6873$, $P > 0.05$). *B*: Representative images of adipose histology demonstrating increased lipid droplets in BAT and decreased multilocular cells in iWAT from mice deficient for *Ire1α* in *Pomc* neurons (chow diet). *C*: Blots represent changes in iWAT UCP1 protein levels in response to cold exposure (chow diet). *$P < 0.05$.

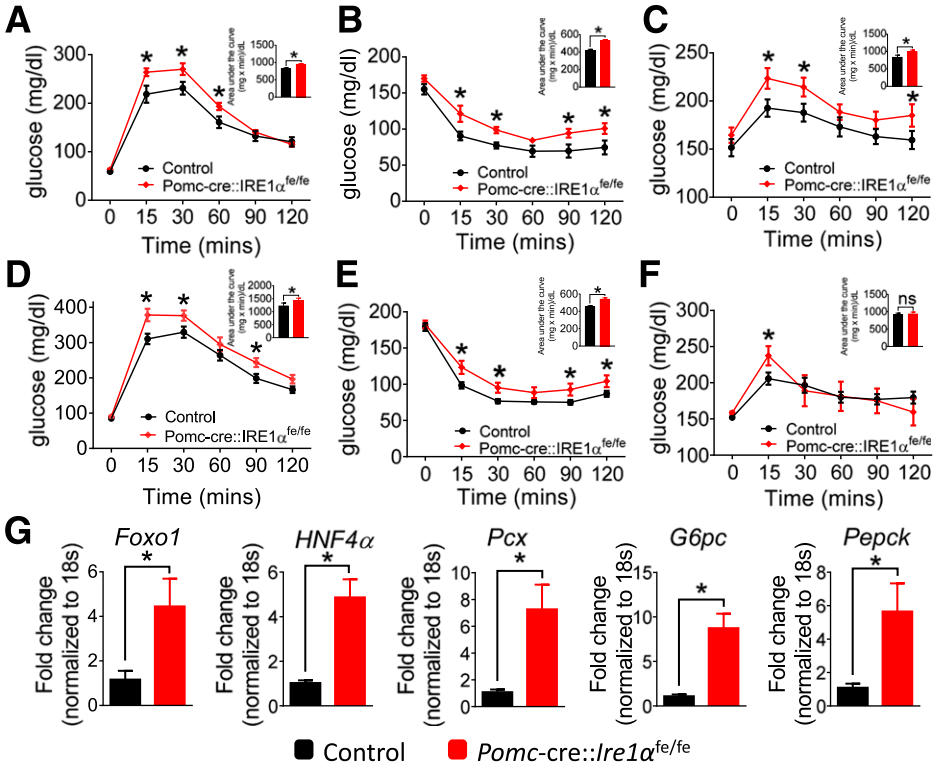

Figure 4—Impaired glucoregulation in mice deficient for *Ire1α* in *Pomc* neurons. Plots for glucose tolerance tests, insulin tolerance tests, and PTTs (area under the curve inset) respectively from *Pomc*-cre::*Ire1α*$^{fe/fe}$ mice and wild-type littermates on a chow diet (*A–C*) or an HFD (*D–F*). *G*: Livers were collected from *Pomc*-cre::*Ire1α*$^{fe/fe}$ mice and wild-type littermates on a chow diet. qPCR was performed to examine the relative expression of *Foxo1*, *Hnf4α*, *Pcx*, *G6pc*, and *Pepck*, which are genes associated with glucose production in the liver. *$P < 0.05$.

exogenous glucose infusion rate (GIR) (Fig. 5*D*). The required GIR during the steady-state period (t = 80–120 min) was lower in *Pomc*-cre::*Ire1α*$^{fe/fe}$ mice, indicating impaired insulin sensitivity (Fig. 5*D*). This was due to impaired insulin-mediated suppression of endogenous glucose appearance (endoR_a) (Fig. 5*E*). There were no significant differences in insulin-stimulated glucose disappearance (R_d) (Fig. 5*F*). Together these data suggest that Pomc neurons selectively deficient for *Ire1α* are linked to impaired insulin sensitivity, which may contribute to hyperglycemia.

Pomc-Specific *Ire1α* Deficiency Accelerates ER Stress–Induced Leptin and Insulin Resistance

Upregulation of the *Ire1α-Xbp1s* pathway in *Pomc* neurons mimics a postprandial state and improves metabolism via a *Ptp1b*/*Socs3*-dependent mechanism (17). Oppositely, the current study suggests that loss of this pathway impairs energy balance and glucose metabolism. However, whether an inverse ER stress–dependent mechanism is also present remains unclear. Deficiency of *Ire1α* in *Pomc* neurons induced *Bip*, *Ptp1b*, and *Socs3* mRNA within the arcuate nucleus (for *Bip*: $t_{(13)} = 2.241$, $P < 0.05$; for *Ptp1b*: $t_{(13)} = 1.924$, $P > 0.05$; for *Socs3*: $t_{(13)} = 2.375$, $P < 0.05$) (Fig. 6), supporting the hypothesis that *Pomc*-cre::*Ire1α*$^{fe/fe}$ mice display increased basal ER stress.

We previously demonstrated that chemical activation of ER stress (6 h) in the arcuate nucleus results in acute leptin and insulin resistance of arcuate *Pomc* neurons (17). We hypothesized that the amplified basal ER stress present in the arcuate nucleus of *Pomc*-cre::*Ire1α*$^{fe/fe}$ mice may result in an increased susceptibility to ER stress–induced leptin and insulin resistance. Whole-cell recordings were performed on acute hypothalamic slices containing *Pomc*-hrGFP neurons within the arcuate nucleus (17,26,27). Similar to previous results (17), leptin depolarized while insulin hyperpolarized subsets of *Pomc* neurons within the arcuate nucleus (Fig. 7*A–F* and Fig. 8*A*). Moreover, *Pomc* neurons from *Pomc*-cre::*Ire1α*$^{fe/fe}$ mice demonstrated analogous acute cellular responses to leptin and insulin (Fig. 7*G* and Fig. 8*B*). Pretreatment of arcuate slices with tunicamycin (30 μmol/L, 1 h) from wild-type *Pomc*-GFP mice failed to alter the acute leptin ($t_{(13)} = 0.6021$, $P > 0.05$) (Fig. 7*F*) and insulin ($t_{(14)} = 1.369$, $P > 0.05$) (Fig. 8*B*) induced changes in membrane potential. Importantly, pretreatment of arcuate slices with tunicamycin (30 μmol/L, 1 h) from *Pomc*-cre::*Ire1α*$^{fe/fe}$ mice was sufficient to abrogate the ability of leptin ($t_{(14)} = 5.708$, $P < 0.05$) (Fig. 7*G*) or insulin ($t_{(14)} = 5.677$, $P < 0.05$) (Fig. 8*B*) to alter the membrane potential of arcuate *Pomc* neurons. Pretreatment of tunicamycin alone failed to alter the resting membrane potential and

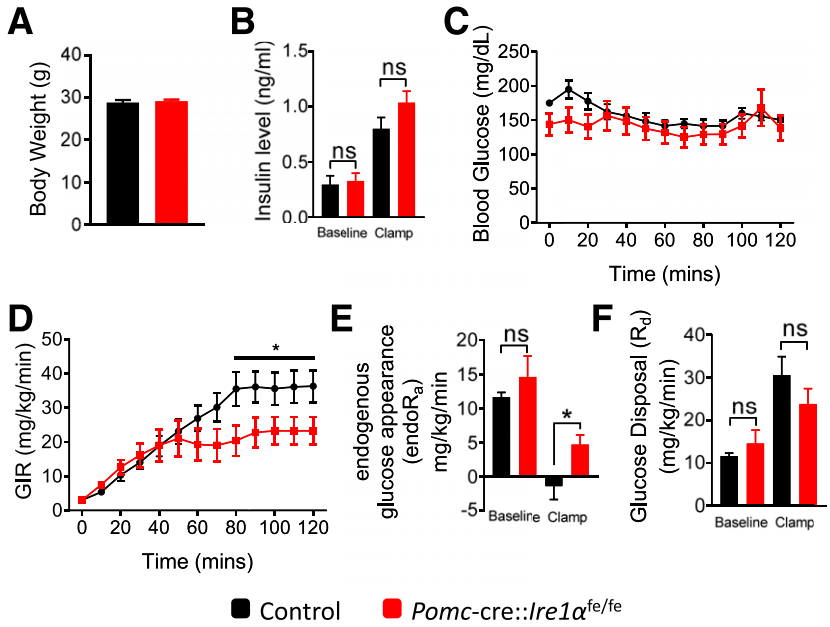

Figure 5—Impaired insulin sensitivity in 5 h–fasted mice lacking *Ire1α* in Pomc neurons. Body weight (*A*), basal and clamp plasma insulin (*B*), and blood glucose (*C*) during a 120-min hyperinsulinemic (2.5 mU/kg/min)-euglycemic (150 mg/dL) clamp in chronically catheterized, conscious, unrestrained mice (n = 8–10/group). *D*: Exogenous GIR needed to clamp blood glucose. *E* and *F*: Basal and clamp endogenous rates of glucose appearance ($endoR_a$) and disappearance (R_d) determined using a constant infusion of [3,4-$^{13}C_2$]glucose to determine plasma M+2 glucose enrichment measured by liquid chromatography–tandem mass spectrometry. Blood samples were taken from the cut tail, and glucose was measured using a commercial glucometer. *$P < 0.05$ and error bars indicate SEM.

excitability of *Pomc* neurons (Supplementary Table 1). These data support that *Pomc* neurons deficient for *Ire1α* are predisposed to the desensitizing effects of ER stress on acute leptin and insulin signaling.

DISCUSSION

Although the requirement of *Ire1α* in specific organs and tissues remains incompletely understood, it is of particular interest that deficiency of *Ire1α* in *Pomc* neurons has effects on body weight and glucose homeostasis. In particular, we demonstrate that selective deficiency of *Ire1α* in *Pomc* neurons (*Pomc*-cre::*Ire1α*$^{fe/fe}$ mice) increased sensitivity to diet-induced obesity in mice. The increased body weight was dependent upon a hypometabolic phenotype (decreased energy expenditure and heat production) and increased food intake. Notably, these responses are phenotypic signatures of impaired leptin action within *Pomc* neurons (28–31). These data were supported by the reduced efficacy of leptin-induced hypophagia as well as the increased susceptibility of ER stress–induced acute leptin and insulin resistance in mice with *Pomc*-specific deficiency of *Ire1α*. The hypometabolic phenotype was also accompanied by decreased markers for thermogenesis in BAT, which suggests that *Ire1α* deficiency in *Pomc* neurons impairs compensatory thermogenesis in response to an HFD and may be a contributing factor in increased body weight. Similar to *Xbp1s* activity in the liver or *Pomc* neurons (17,22), we also found that deficiency of *Ire1α* in *Pomc* neurons alone was sufficient to impair blood glucose and insulin levels (e.g., impaired glucose/insulin tolerance, increased gluconeogenic expression/PTT response, increased GSIS, and reduced hepatic insulin sensitivity) independent of changes in body weight. On a cellular level, *Pomc*-cre::*Ire1α*$^{fe/fe}$ mice exhibited increased basal ER stress in the arcuate nucleus, contributing to an amplified sensitivity to ER stress–dependent leptin and insulin resistance. Together, these data support a model in which loss of *Ire1α* in *Pomc* neurons accelerates HFD-induced obesity while at the same time impairing glucose homeostasis.

This study reinforces an important relationship between *Ire1α-Xbp1s* and *Ptp1b/Socs3* in the ER stress–induced acute leptin and insulin resistance of arcuate *Pomc* neurons. In particular, both *Socs3* and *Ptp1b* are increased within the hypothalamus in a state of excess nutrition or obesity (32–36). Moreover, there is a fundamental role of ER stress in regulating leptin and insulin signaling in hypothalamic *Pomc* neurons via a *Ptp1b/Socs3*-dependent mechanism (17). In particular, transcripts of both *Ptp1b* and *Socs3* were also lowered in mice with constitutive activation of *Xbp1s* in *Pomc* neurons (17). *Pomc* neurons selectively deficient for either *Ptp1b* or *Socs3* also demonstrated improved acute leptin and insulin signaling even in the presence of strong activators of ER stress (17). These data were supported in the current study by the inverse finding that *Pomc*-specific deficiency of *Ire1α*

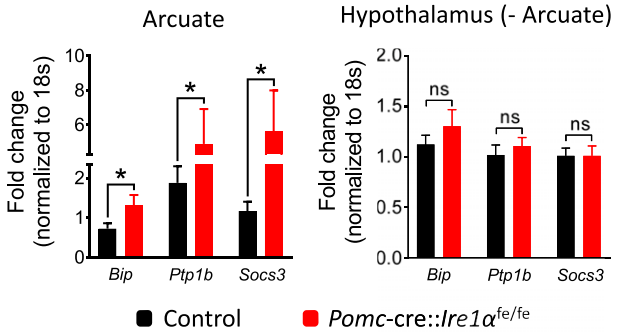

Figure 6—Regulation of *Bip*, *Ptp1b*, and *Socs3* in the arcuate nucleus and the remaining hypothalamus. qPCR was performed on mice chronically fed an HFD to examine the relative expression of *Bip*, *Ptp1b*, *and Socs3*. *$P < 0.05$ compared with control (wild-type littermates). Fold change is relative to 18S mRNA. n = 4–8 per group. Error bars indicate SEM.

stimulates *Ptp1b* and Socs3 in the arcuate nucleus of the hypothalamus. This also correlated with a decreased sensitivity to pharmacological leptin-induced hypophagia as well as at the cellular level an increased susceptibility to ER stress–dependent acute leptin and insulin resistance. These data support a *Ptp1b/Socs3*-dependent, ER stress–induced acute leptin and insulin resistance in the absence of *Ire1-Xbp1* activation.

Another salient finding is the suggestion that the *Ire1α-Xbp1s* pathway in *Pomc* neurons is required and sufficient (17) for diet- and cold-induced thermogenesis in iBAT and "browning" of iWAT, respectively. This is topical given that activation of functional iBAT depots in adult humans (37–40) as well as induction of thermogenic programs in WAT (41,42) has recently emerged as a potential therapeutic approach in the treatment of obesity and diabetes (43). However, it is important to clarify that our data cannot firmly establish that defects in iBAT and/or ability to "brown" iWAT contribute to altered energy expenditure, body weight, and/or glycemia in mice. In fact, mice deficient for *Ire1α* in *Pomc* neurons exhibited decreased thermogenic markers in BAT independent of changes in body weight on a chow diet. However, when exposed to an HFD, the defects in thermogenesis of BAT were greatly exaggerated. Moreover, transgenic overexpression of the *Ire1α-Xbp1s* pathway in *Pomc* neurons increased thermogenesis of BAT and iWAT concomitant with a protection against diet-induced obesity independent of changes in food intake (17). Thus, although it is

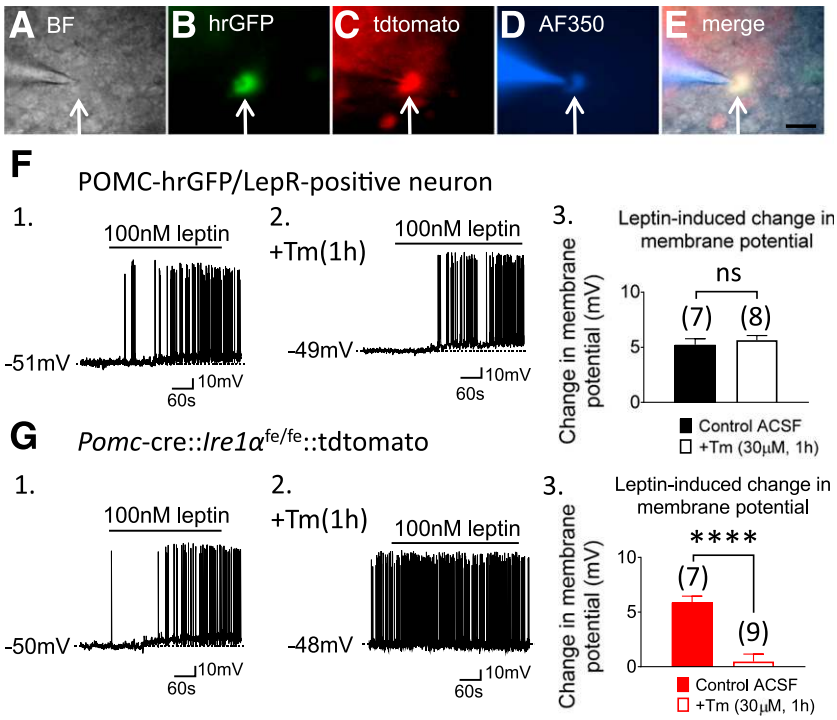

Figure 7—Pretreatment with tunicamycin (Tm) abrogated the leptin-induced activation of *Pomc* neurons deficient for *Ire1α*. Brightfield (BF) illumination (*A*) of a Pomc-hrGFP neuron from a GFP-labeled mouse. The same neuron under fluorescein isothiocyanate (hrGFP), tdtomato, and Alexa Fluor 350 (AF350) illumination is shown in *B*, *C*, and *D*. The merged image of the targeted Pomc neuron is shown in *E*. Arrow indicates the targeted cell. Scale bar = 50 μm. *F*: Electrophysiological recording demonstrates that leptin depolarized arcuate Pomc-hrGFP (green) neurons from *Pomc*-hrGFP::*LepR*-cre::tdtomato mice in the control group (1) and Tm-incubated group (2). Dashed line indicates the resting membrane potential. Histogram shows the leptin-induced change in membrane potential from control and Tm (30 μmol/L, 1 h)-incubated group (3). *G*: Representative traces show that *Pomc* neurons from *Pomc*-cre::*Ire1α*$^{fe/fe}$::tdtomato mice are depolarized by leptin in the control group (1) yet fail to respond to leptin when pretreated with Tm (30 μmol/L) for 1 h (2). Dashed line indicates the resting membrane potential. Leptin-induced change in membrane potential from control and Tm-treated groups are shown in panel 3. ****$P < 0.001$.

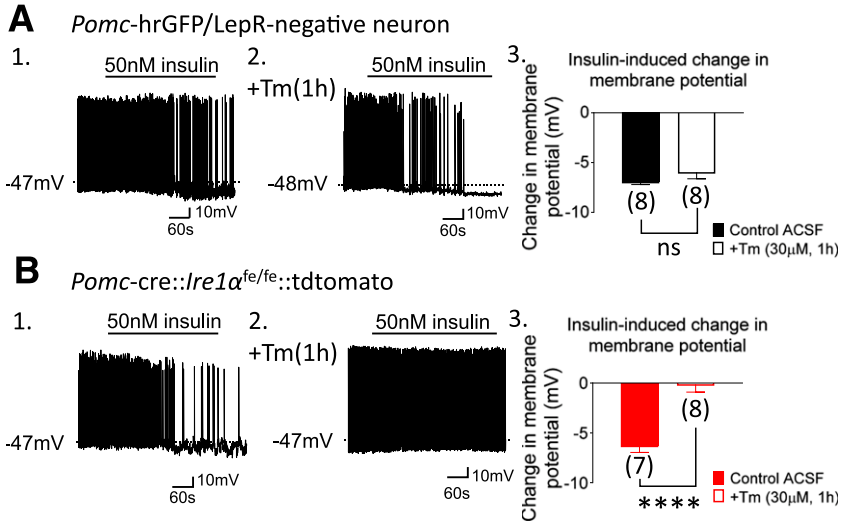

Figure 8—Deletion of *Ire1α* from *Pomc* neurons accelerated the acute insulin resistance in *Pomc* neurons. *A*: Current-clamp recording demonstrates that insulin hyperpolarized arcuate Pomc neurons from *Pomc*-hrGFP::*LepR*-cre::tdtomato mice in the control (1) and tunicamycin (Tm)-pretreated (2) groups. Dashed line indicates the resting membrane potential. Histogram shows the insulin-induced change in membrane potential from control and Tm-incubated groups (3). *B*: Representative traces illustrate an insulin-induced hyperpolarization of *Pomc* neurons from *Pomc*-cre::*Ire1α*::tdtomato mice (1) and that Tm pretreatment (2) blocks the insulin-induced hyperpolarization of *Pomc* neurons from the same mouse. Insulin-induced changes in membrane potential from control and Tm-pretreatment groups are shown in panel 3. ****$P < 0.001$.

difficult to determine the independent contribution of energy intake versus energy expenditure resulting in weight gain, the *Ire1α-Xbp1s* pathway in *Pomc* neurons consistently modifies thermogenic programs that may underlie deficits associated with obesity.

The current study also highlights an important transient regulation of leptin and potentially insulin signaling within arcuate *Pomc* neurons. In particular, leptin signaling within *Pomc* neurons is necessary and sufficient to regulate proper energy and glucose homeostasis (28,29). Although insulin signaling alone in *Pomc* neurons minimally alters energy balance or glucose metabolism, loss of both leptin and insulin signaling results in larger glycemic dysregulation than loss of either receptor alone (44). Chemical activation of ER stress abrogates leptin and insulin signaling within the periphery as well as the CNS (including *Pomc* neurons) (17,21,45). Also, increased basal ER stress as occurs with loss of *Ire1α* in *Pomc* neurons accelerated leptin and insulin resistance. The acute gating of these signaling pathways (both leptin and insulin via a mechanism similar to a rheostat) may contribute to alterations in energy balance and systemic glucose metabolism and insulin sensitivity. Importantly, both *Ire1α* and *Xbp1s* are regulated depending on various metabolic states (17,22,46). Thus, this may highlight an important conserved mechanism that responds to fluctuating energy demands, independent of altered leptin and insulin levels. It is important to note that in addition to the role of *Ire1α* in the regulation of Xbp1s activity, *Ire1α* has additional endonuclease and intrinsic kinase activity that ultimately facilitates recovery from ER stress (47–50). Although the current study supports a model demonstrating a requirement of the *Ire1α-Xbp1s* pathway in the protection from obesity and diabetes, we cannot exclude the possibility that additional activities of *Ire1α* (endonuclease or intrinsic kinase activity) may contribute to the metabolic phenotypes observed in the current study. Moreover, the age dependence of the body weight phenotype as well as the tunicamycin-dependent blunting of acute leptin and insulin signaling in arcuate Pomc neurons may suggest the requirement of a "trigger" in order to elicit changes in metabolism. Several triggers could be sufficient to drive these processes, including aging and HFD (both of which can precipitate hypothalamic ER stress).

Overall, these findings extend the physiologically important role of ER stress and the UPR in *Pomc* neurons to regulate sensitivity to humoral signals, ultimately contributing to diet-induced obesity and diabetes. Notably, *Ptp1b* and *Socs3* are reciprocally regulated in response to altered *Ire1α-Xbp1s* signaling, providing a potential molecular link between ER stress and leptin/insulin resistance. Together, these data highlight multiple molecular targets that may contribute to obesity and diabetes.

Acknowledgments. The authors thank Dr. Joel K. Elmquist (Division of Hypothalamic Research, Department of Internal Medicine, UTSW Medical Center) for kindly providing the *Pomc*-cre and *Pomc*-hrGFP mice.

Funding. This work was supported by grants to T.Y. (China Scholarship Council 201406280111), J.S. (National Natural Science Foundation of China 81300689 and 81670783), X.K. (National Institute of Diabetes and Digestive and

Kidney Diseases [NIDDK] 5K99DK106550), E.D.B. (NIDDK R01 DK109408), R.J.K. (NIDDK R37 DK042394, R24 DK110973, R01 DK103825, and R01 DK103185), T.L. (American Heart Association 14SDG20370016), and K.W.W. (NIDDK R01 DK100699). This work was also supported by NIDDK PL1 grant DK081182 and National Institutes of Health grant UL1RR024923.

Duality of Interest. No potential conflicts of interest relevant to this article were reported.

Author Contributions. T.Y., Z.D., and J.S. designed and performed all experiments except immunoblotting, analyzed the data, and wrote the manuscript. Y.G. performed electrophysiological experiments, analyzed data, and wrote the manuscript. X.K. analyzed gene expression in adipose depots, performed immunoblotting in BAT, analyzed the data, and reviewed the manuscript. Y.H., Z.H., and Y.X. assisted in performing experiments. Y.C., K.-j.Y., R.-t.W., H.G., H.C., and X.L. designed experiments and edited the manuscript. B.G.F. performed hyperinsulinemic-euglycemic clamps and analyzed the data. E.D.B. designed and performed hyperinsulinemic-euglycemic clamp experiments, analyzed the data, and reviewed the manuscript. R.J.K. designed and developed the *IRE1α*$^{fe/fe}$ mouse and edited the manuscript. J.Y. and T.L. supervised development of the mouse models, designed experiments, and edited the manuscript. K.W.W. conceived and designed the study, supervised development of the mouse models, designed experiments, and edited the manuscript. K.W.W. is the guarantor of this work and, as such, had full access to all the data in the study and takes responsibility for the integrity of the data and the accuracy of the data analysis.

References

1. Ron D, Walter P. Signal integration in the endoplasmic reticulum unfolded protein response. Nat Rev Mol Cell Biol 2007;8:519–529
2. Ma Y, Hendershot LM. The unfolding tale of the unfolded protein response. Cell 2001;107:827–830
3. Wang M, Kaufman RJ. Protein misfolding in the endoplasmic reticulum as a conduit to human disease. Nature 2016;529:326–335
4. Ozcan L, Ergin AS, Lu A, et al. Endoplasmic reticulum stress plays a central role in development of leptin resistance. Cell Metab 2009;9:35–51
5. Ozcan U, Cao Q, Yilmaz E, et al. Endoplasmic reticulum stress links obesity, insulin action, and type 2 diabetes. Science 2004;306:457–461
6. Milanski M, Degasperi G, Coope A, et al. Saturated fatty acids produce an inflammatory response predominantly through the activation of TLR4 signaling in hypothalamus: implications for the pathogenesis of obesity. J Neurosci 2009;29:359–370
7. Zhang X, Zhang G, Zhang H, Karin M, Bai H, Cai D. Hypothalamic IKKbeta/NF-kappaB and ER stress link overnutrition to energy imbalance and obesity. Cell 2008;135:61–73
8. Hotamisligil GS. Role of endoplasmic reticulum stress and c-Jun NH2-terminal kinase pathways in inflammation and origin of obesity and diabetes. Diabetes 2005;54(Suppl. 2):S73–S78
9. Rao RV, Bredesen DE. Misfolded proteins, endoplasmic reticulum stress and neurodegeneration. Curr Opin Cell Biol 2004;16:653–662
10. Schröder M, Kaufman RJ. ER stress and the unfolded protein response. Mutat Res 2005;569:29–63
11. Shen X, Zhang K, Kaufman RJ. The unfolded protein response–a stress signaling pathway of the endoplasmic reticulum. J Chem Neuroanat 2004;28:79–92
12. Harding HP, Zhang Y, Ron D. Protein translation and folding are coupled by an endoplasmic-reticulum-resident kinase. Nature 1999;397:271–274
13. Shi Y, Vattem KM, Sood R, et al. Identification and characterization of pancreatic eukaryotic initiation factor 2 alpha-subunit kinase, PEK, involved in translational control. Mol Cell Biol 1998;18:7499–7509
14. Lee K, Tirasophon W, Shen X, et al. IRE1-mediated unconventional mRNA splicing and S2P-mediated ATF6 cleavage merge to regulate XBP1 in signaling the unfolded protein response. Genes Dev 2002;16:452–466
15. Zhang K, Wong HN, Song B, Miller CN, Scheuner D, Kaufman RJ. The unfolded protein response sensor IRE1alpha is required at 2 distinct steps in B cell lymphopoiesis. J Clin Invest 2005;115:268–281
16. Reimold AM, Etkin A, Clauss I, et al. An essential role in liver development for transcription factor XBP-1. Genes Dev 2000;14:152–157
17. Williams KW, Liu T, Kong X, et al. Xbp1s in Pomc neurons connects ER stress with energy balance and glucose homeostasis. Cell Metab 2014;20:471–482
18. Hill JW, Williams KW, Ye C, et al. Acute effects of leptin require PI3K signaling in hypothalamic proopiomelanocortin neurons in mice. J Clin Invest 2008;118:1796–1805
19. Ayala JE, Samuel VT, Morton GJ, et al.; NIH Mouse Metabolic Phenotyping Center Consortium. Standard operating procedures for describing and performing metabolic tests of glucose homeostasis in mice. Dis Model Mech 2010;3:525–534
20. Heikkinen S, Argmann CA, Champy MF, Auwerx J. Evaluation of glucose homeostasis. Curr Protoc Mol Biol 2007;Chapter 29:Unit 29B.3
21. Ozcan U, Yilmaz E, Ozcan L, et al. Chemical chaperones reduce ER stress and restore glucose homeostasis in a mouse model of type 2 diabetes. Science 2006;313:1137–1140
22. Deng Y, Wang ZV, Tao C, et al. The Xbp1s/GalE axis links ER stress to postprandial hepatic metabolism. J Clin Invest 2013;123:455–468
23. Zhang K, Wang S, Malhotra J, et al. The unfolded protein response transducer IRE1α prevents ER stress-induced hepatic steatosis. EMBO J 2011;30:1357–1375
24. Dodd GT, Decherf S, Loh K, et al. Leptin and insulin act on POMC neurons to promote the browning of white fat. Cell 2015;160:88–104
25. Berglund ED, Liu T, Kong X, et al. Melanocortin 4 receptors in autonomic neurons regulate thermogenesis and glycemia. Nat Neurosci 2014;17:911–913
26. Parton LE, Ye CP, Coppari R, et al. Glucose sensing by POMC neurons regulates glucose homeostasis and is impaired in obesity. Nature 2007;449:228–232
27. Ramadori G, Fujikawa T, Fukuda M, et al. SIRT1 deacetylase in POMC neurons is required for homeostatic defenses against diet-induced obesity. Cell Metab 2010;12:78–87
28. Balthasar N, Coppari R, McMinn J, et al. Leptin receptor signaling in POMC neurons is required for normal body weight homeostasis. Neuron 2004;42:983–991
29. Berglund ED, Vianna CR, Donato J Jr, et al. Direct leptin action on POMC neurons regulates glucose homeostasis and hepatic insulin sensitivity in mice. J Clin Invest 2012;122:1000–1009
30. Williams KW, Scott MM, Elmquist JK. Modulation of the central melanocortin system by leptin, insulin, and serotonin: co-ordinated actions in a dispersed neuronal network. Eur J Pharmacol 2011;660:2–12
31. Huo L, Gamber K, Greeley S, et al. Leptin-dependent control of glucose balance and locomotor activity by POMC neurons. Cell Metab 2009;9:537–547
32. Bjørbaek C, Elmquist JK, Frantz JD, Shoelson SE, Flier JS. Identification of SOCS-3 as a potential mediator of central leptin resistance. Mol Cell 1998;1:619–625
33. Enriori PJ, Evans AE, Sinnayah P, et al. Diet-induced obesity causes severe but reversible leptin resistance in arcuate melanocortin neurons. Cell Metab 2007;5:181–194
34. Münzberg H, Flier JS, Bjørbaek C. Region-specific leptin resistance within the hypothalamus of diet-induced obese mice. Endocrinology 2004;145:4880–4889
35. White CL, Whittington A, Barnes MJ, Wang Z, Bray GA, Morrison CD. HF diets increase hypothalamic PTP1B and induce leptin resistance through both leptin-dependent and -independent mechanisms. Am J Physiol Endocrinol Metab 2009;296:E291–E299

36. Zabolotny JM, Bence-Hanulec KK, Stricker-Krongrad A, et al. PTP1B regulates leptin signal transduction in vivo. Dev Cell 2002;2:489–495
37. Cypess AM, Lehman S, Williams G, et al. Identification and importance of brown adipose tissue in adult humans. N Engl J Med 2009;360:1509–1517
38. Mirbolooki MR, Constantinescu CC, Pan ML, Mukherjee J. Quantitative assessment of brown adipose tissue metabolic activity and volume using ^{18}F-FDG PET/CT and β3-adrenergic receptor activation. EJNMMI Res 2011; 1:30
39. Virtanen KA, Lidell ME, Orava J, et al. Functional brown adipose tissue in healthy adults. N Engl J Med 2009;360:1518–1525
40. Orava J, Nuutila P, Lidell ME, et al. Different metabolic responses of human brown adipose tissue to activation by cold and insulin. Cell Metab 2011;14:272–279
41. Zhan C, Zhou J, Feng Q, et al. Acute and long-term suppression of feeding behavior by POMC neurons in the brainstem and hypothalamus, respectively. J Neurosci 2013;33:3624–3632
42. Tseng YH, Cypess AM, Kahn CR. Cellular bioenergetics as a target for obesity therapy. Nat Rev Drug Discov 2010;9:465–482
43. Nedergaard J, Cannon B. The browning of white adipose tissue: some burning issues. Cell Metab 2014;20:396–407
44. Hill JW, Elias CF, Fukuda M, et al. Direct insulin and leptin action on pro-opiomelanocortin neurons is required for normal glucose homeostasis and fertility. Cell Metab 2010;11:286–297
45. Schneeberger M, Dietrich MO, Sebastián D, et al. Mitofusin 2 in POMC neurons connects ER stress with leptin resistance and energy imbalance. Cell 2013;155:172–187
46. Lee AH, Glimcher LH. Intersection of the unfolded protein response and hepatic lipid metabolism. Cell Mol Life Sci 2009;66:2835–2850
47. Hollien J, Weissman JS. Decay of endoplasmic reticulum-localized mRNAs during the unfolded protein response. Science 2006;313:104–107
48. Han D, Lerner AG, Vande Walle L, et al. IRE1alpha kinase activation modes control alternate endoribonuclease outputs to determine divergent cell fates. Cell 2009;138:562–575
49. Oikawa D, Tokuda M, Hosoda A, Iwawaki T. Identification of a consensus element recognized and cleaved by IRE1 alpha. Nucleic Acids Res 2010;38: 6265–6273
50. Hollien J, Lin JH, Li H, Stevens N, Walter P, Weissman JS. Regulated Ire1-dependent decay of messenger RNAs in mammalian cells. J Cell Biol 2009;186: 323–331